Journal of Thermal Engineering
https://jten.yildiz.edu.tr/
https://doi.org/10.47481/jten.0054

RESEARCH ARTICLE

Analyzing the impact of plate integration on the thermal and flow performance of microchannel heat sinks

Anas Khan[1], Mahmood Alam[2,3,*], Mohammad Nawaz Khan[4], Mohd. Anas [5], Abhishek Dwivedi[6]

[1]Department of Mechanical Engineering, Integral University, Lucknow, 226026, India
[2]Department of Mechanical Engineering, Integral University, Lucknow, 226026, India
[3]Mechanical Engineering Department, Indian Institute of Technology (Indian School of Mines), Dhanbad, 826004, India
[4]Department of Mechanical Engineering, Integral University, Lucknow, 226026, India
[5]Department of Mechanical Engineering, Integral University, Lucknow, 226026, India
[6]Department of Mechanical Engineering, Integral University, Lucknow, 226026, India

Abstract

This study investigates the thermal and fluid-flow performance of three microchannel heat-sink configurations: simple rectangular (plain), triangular edge-plate, and zigzag edge-plate. This study aims to cool high-power-density processors, specifically the Intel Core i5-7600K. The processor has a thermal design power of 91 W and a compact die size of about 100 mm². These conditions create significant thermal challenges, requiring efficient and compact cooling strategies. The study uses numerical simulations across a range of Reynolds numbers. It evaluates key performance parameters such as the Nusselt number and the convective heat transfer coefficient. Pressure drop and the thermal performance factor are also analyzed. The results indicate that the plain microchannel has the lowest pressure drop but the poorest thermal performance due to limited boundary-layer disturbance. The triangular edge-plate configuration enhances heat transfer through secondary flow generation, achieving a moderate thermal performance factor of 1.15. In contrast, the zigzag edge-plate design delivers the highest thermal performance factor of 1.20, with heat transfer coefficients increasing by 32.01%–38.21% relative to the plain configuration. Although this improvement incurs a pressure-drop penalty, the zigzag channel still consistently outperforms the other designs, achieving up to 11.77% better performance than that of the triangular geometry at low Reynolds numbers. This study presents a novel geometric approach to MCHS optimization through internal plate integration, offering valuable insights into developing compact, high-efficiency thermal management solutions for next-generation electronic systems.

Keywords: Microchannel Heat sink (MCHS), Thermal Performance factor (TPF), pressure drop, nusselt number, heat transfer

Cite this article as: Khan, A., Alam, M., Khan, M. N., Anas, M., & Dwivedi, A. (2026). Analyzing the impact of plate integration on the thermal and flow performance of microchannel heat sinks. Journal of Thermal Engineering, 12(5), 1641–1654. https://doi.org/10.47481/jten.0054

1. Introduction

The fast-paced growth of microelectronics has increased the demand for compact thermal management systems. Excessive heat reduces performance and shortens the lifespan of components. Hanafi et al. [1] identified overheating as a major cause of electronic failure. V. Lakshminarayanan et al. [2] discussed its impact on reliability and suggested strategies to reduce thermal stress. Momen S. M. Saleh et al. [3] also reported that high operating temperatures hinder CPU performance. The concept of microchannel heat sinks (MCHS) was first introduced by Tuckerman and Pease [4] for VLSI cooling. Since then, numerous improvements have been made through advances in geometry and materials. Dwight Cooke et al. [5] demonstrated that structured microchannels enhance pool boiling by a factor of 3.4. Robert Kaniowski et al. [6] highlighted the importance of channel depth in nucleate boiling. Arvind Jaikumar et al. [7] achieved high performance with selectively sintered microchannels, reporting a CHF of 420 W/cm² and an HTC of 2.9 MW/m²°C. Apart from geometric considerations, researchers have focused on advanced coolants. Y. Khan et al. [8] demonstrated that GaIn–CNT nanofluids improve thermal

*Corresponding Author
E-mail Adress: mahmood@iul.ac.in

Submitted: 13 June 2025; **Accepted:** 9 September 2025

This paper was recommended for publication in revised form by Editor-in-Chief Ahmet Selim Dalkılıç

Published by Yıldız Technical University, İstanbul, Türkiye

performance more than 3.4 times compared to water-based nanofluids. B. Jalili et al. [9] combined Al_2O_3 nanofluids with curved fins and achieved higher heat transfer efficiency. Chunyang Li et al. [10] studied hybrid nanofluids (Al_2O_3 + Cu + H_2O) and reported better flow velocity and heat distribution. A. Belhadj et al. [11] confirmed that water/Al_2O_3 nanofluids improve both thermal transport and frictional behaviour, especially at higher concentrations and Reynolds numbers.

Comparative designs have also been explored to improve the performance of microchannel heat sinks. H.A. Mohammed et al. [12] studied zigzag channels and found superior heat transfer but with high pressure drops. Ankur Sharma et al. [13] showed that elliptical-wavy channels generally perform better than sinusoidal ones. Eltaweel et al. [14] further demonstrated that optimized wavy-tapered channels reduce thermal resistance by up to 15%. M. Zunaid et al. [15] numerically analyzed rectangular and semi-cylindrical channels and reported better performance for semi-cylindrical designs. These studies demonstrate that both geometry and coolant selection are crucial for enhancing the thermal-hydrodynamic performance of microchannel heat sinks in high-performance electronics.

Recent advancements in microchannel heat sink (MCHS) design have emphasized improving thermal performance by incorporating ribs, grooves, and fins that induce flow obstruction. B. Jalili et al. [16] reported that obstruction enhances turbulence and vortex energy storage, while D. Salehipour et al. [17] examined spiral geometries, showing their role in improving heat transfer. Similarly, P. Jalili and B. Jalili [18] introduced turbulators to intensify turbulence, thereby increasing efficiency. Lei Chai et al. [19] developed a 3D optimization model for rib size and placement, generating performance maps to balance pressure drop and heat transfer. Building on this, Ihsan Ali Ghani et al. [20] showed that the MC-SOCRR design with oblique secondary channels (k=0.666, b=0.5, θ=45°) yields optimal thermal-hydraulic performance, while Guilian Wang et al. [21] demonstrated that bidirectional ribs enhance heat transfer 1.2–2 times, albeit with added pressure drop. V. P. Gaikwad et al. [22] proposed secondary channels, reporting a performance factor of 1.4–1.85. Qifeng Zhu et al. [23] achieved a fourfold enhancement via wavy microchannels with ribs, highlighting synergy from combined geometries. Liang Du et al. [24] showed square orthogonal ribs in diamond channels increased heat transfer by 182.8% at PEC = 1.92, while Alişan and Abdulkerim [25] achieved up to 230% improvement using vortex generators (JF = 1.38). Complementary studies by Naushad Ali et al. [26] on V-ribs (35°) and Fadi Alnaimat et al. [27] on triangular ribs (71% thermal resistance reduction) confirmed that rib-based designs significantly improve thermal performance but require careful optimization due to pumping power penalties.

Parallel research has focused on grooves to enhance conduction. Navin Raja Kuppusamy et al. [28] and Hamdi E. Ahmed et al. [29] demonstrated that trapezoidal grooves with Al_2O_3-H_2O nanofluids optimize performance. Extending this, P. Jalili et al. [30] employed alumina-Cu-water hybrid nanofluids, reporting 84% heat transfer enhancement, while S. L. Sun et al. [31] showed Fe_3O_4 suspensions under magnetic fields further improved heat transfer, revealing a controllable pathway. Qifeng Zhu et al. [32] found triangular grooves most effective, while water-droplet grooves delivered optimum overall efficiency. Pankaj Kumar et al. [33] noted the minimal effect of groove offset but developed an empirical prediction correlation. Qinghua Wang et al. [34] combined fan-shaped grooves with truncated triangular ribs, achieving a performance factor of 1.081. Lin Liu et al. [35] reported staggered triangular grooves with PEC = 1.61, while Bin Li et al. [36] studied a slant rib-elliptical groove–quatrefoil rib structure, achieving 52.3% temperature reduction and 131% higher Nusselt number at Re = 696. Finally, Yifan Li et al. [37] optimized offset grooves, achieving a 10.52× improvement in heat transport and 71.47% pumping power reduction. Collectively, these studies underscore that ribs and grooves are versatile design strategies for advanced MCHS, with performance dictated by geometry, orientation, and integration.

Several studies have focused on optimizing fins and ribs as extended surfaces to improve heat conduction efficiency in microchannel heat sinks (MCHSs). V. P. Gaikwad and S. S. Mohite [38] investigated pin-enhanced MCHSs and reported optimal performance with 0.2 mm pins, achieving an average enhancement factor of 1.24. Liu et al. [39] showed that square pin fins enable up to 2.83 MW/m^2 cooling capacity, with Nusselt number and pressure drop rising as Reynolds number increases. Jani and Saeid [40] further confirmed that in-fin microchannels deliver superior heat dissipation at higher Reynolds numbers. O. O. Adewumi et al. [41] optimized 3D pin-fin MCHSs and identified peak thermal performance with 3–6 fin rows, owing to minimized wall temperatures and maximized conductance. Turker et al. [42] revealed that rectangular pin fins provide the highest heat transfer, whereas cone-shaped fins offer better overall thermal-hydraulic performance. Similarly, Yu et al. [43] introduced Piranha Pin Fin (PPF) microchannels, achieving 676 W/cm^2 critical heat flux, demonstrating effective cooling with manageable pressure drop in flow boiling. Yuting Jia et al. [44] found that uniformly distributed cone-shaped fins yield balanced thermal and hydraulic performance.

Jingzhe Xie et al. [45] highlighted the importance of fin spacing, reporting that a gap-to-diameter ratio (G/D) of 1.0 enhances thermal performance by 10–13.5% while preserving hydraulic efficiency. M. O. Qidwai et al. [46] demonstrated that combining microjet impingement with pin fins further enhances cooling. Saqib Ali et al. [47] showed that fan-cavity microchannels with front-and-back ribs increase heat transfer by 19% compared to center-ribbed designs. Mukhtar et al. [48] reported that reduced-height pin fins in open channels increase heat conduction by 16.8% and lower pressure losses by 7.3% compared to closed counterparts. M. N. Khan et al. [49][50] studied perforated pin fins (α = 0.33), where α = D_perf/D_fin, and revealed that perforation location critically affects performance. Nanofluids have also been incorporated into fin-based MCHSs. Tehmina Ambreen et al. [51] showed that circular pin fins combined with nanofluids yield the best thermal performance due to smoother flow and delayed separation. Shuo-Lin Wang et al. [52] demonstrated that porous fins in double-layered channels reduce pumping power through coolant slip effects. Subhash V. Jadhav et al. [53] reported that square fins of 700 µm height achieve the highest Nusselt numbers, while Shuja et al. [54] observed that hydrophilic fins enhance heat transfer, whereas hydrophobic fins lower pressure drop by 6–16%, with performance varying across Reynolds numbers. Prabhakar Bhandari et al. [55] found that 1.5 mm fins in open MCHSs balance heat conduction and pressure drop. Similarly, Omar A. Ismail et al. [56] optimized tapered square fins, achieving an effective balance between resistance and pressure losses.

More innovative approaches include Yunfei Yan et al. [57], who developed the DP-MCHS-PS, reducing pressure drop by 56.3% while improving heat dissipation. M. Alam et al. [58] examined rib–fin integration and reported that two ribs deliver maximum heat transfer, with wider ribs boosting performance up to 25%. Aditya Manoj et al. [59] explored alternative geometries, such as plate structures, enhancing heat transfer through combined convection and conduction. Beyond geometry, the optimization of flow processes has received increasing attention. S. L. Sun et al. [60] applied a GA-assisted BPNN model to predict Taylor–Couette flow, achieving a 16.35% improvement in heat transfer. Likewise, S. Nekahi et al. [61] enhanced finned MCHS performance using coupled numerical simulation, artificial neural networks, and multi-objective optimization. Finally, A. Rabiee et al. [62] applied the NSGA-II algorithm to optimize rectangular MCHSs, reducing entropy generation while improving hydrothermal efficiency. Together, these studies highlight the importance of geometric refinement, material integration, and intelligent optimization in advancing the design of high-performance fin- and rib-enhanced MCHSs.

Many efforts have been made to improve the thermal performance of microchannel heat sinks (MCHSs); common strategies include adding ribs, grooves, and fins, and using nanofluids. However, the role of plate shape variations as internal flow modifiers has not been adequately explored. Prior studies have largely concentrated on conventional geometries and simulation-based optimization, without fully addressing how alternative plate designs can alter flow paths, generate localized turbulence, and disrupt boundary layers. This knowledge gap limits the development of innovative MCHS designs that simultaneously enhance conduction and convection. In this work, we address this gap by introducing plate-shaped microplate designs within a microchannel heat sink. The proposed design is applied to address the overheating of an Intel Core i5-7600K processor. By integrating plates, the heat sink achieves more uniform heat transfer, improved cooling efficiency, and reduced processor temperatures. This not only maintains system reliability and prevents thermal throttling but also extends the processor's lifespan. The novelty of this approach lies in its ability to provide a balanced improvement in thermal performance while incurring lower hydraulic penalties compared with rib-based, groove-based, or wavy-based designs. Furthermore, the plate-integration method is versatile and can be extended to applications in high-performance computing, gaming systems, and other compact electronic devices that require efficient cooling.

2. Physical model illustrating the heat sink geometry and structure

To conduct the simulation study, a unit cell of a 10 mm-long microchannel was isolated from a compact heat sink module (10 mm × 10 mm) composed of 50 parallel channels, as illustrated in Figure 1. The selected microchannel served as the computational model for the analysis. The micro channel was formed within a silicon base block shaped in a rectangular form, with substrate dimensions of the width (Wsb) and height (Hsb) are 500 µm and 700 µm, respectively. The channel itself has a cross-section 250 µm wide (Wch) and 500 µm deep (Hch). Purified water free of ions was employed as the working fluid for cooling. Inside the channel, three plates are evenly spaced along their length, and their geometry is reinforced to enhance performance.

In addition to the plain microchannel, we explored two other designs to assess the heat sink's performance: one comprising a plain channel fitted with triangular-edged plates, and the other featuring zigzag-edged plates. These variations were simulated to assess how they compare with the basic design. The dimensions of the plates are outlined in Table 1.

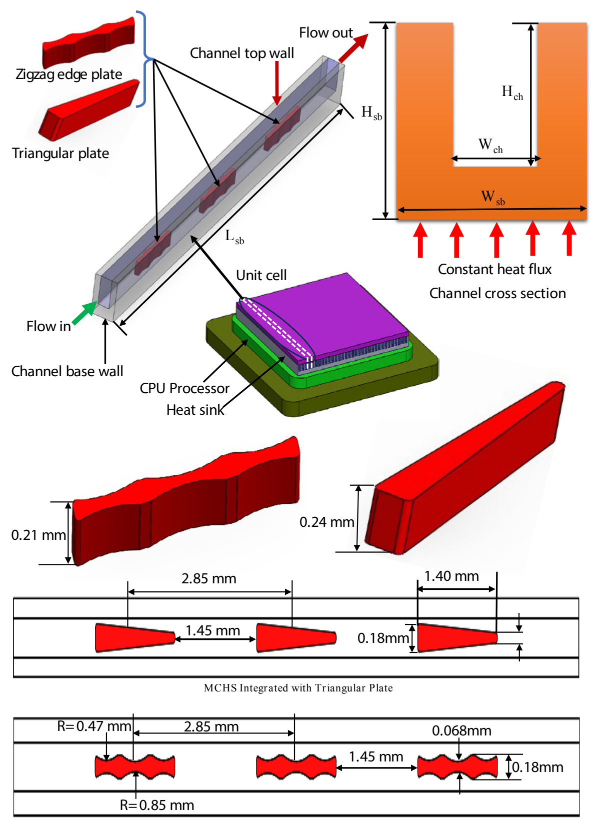

Figure 1. Physical model of computational domain

Table 1. Dimensions of plates integrated with plain channel

Plate design	Height(μm)	Width (μm)	Length (μm)	Surface area (μm^2)	Total Interface area of Plate (μm^2)
Triangular Plate	210	120	1410	960	2850
Zigzag edge	210	120	1410	960	2850

3. Numerical methodology

3.1. Assumptions and core equations for modelling thermofluids analysis

To keep the numerical simulation manageable, the study relies on these assumptions:

1. We applied a stationary-fluid boundary condition at the wall where the fluid contacts solid surfaces, meaning the fluid velocity is zero relative to the wall.
2. The thermophysical properties of the substrate material remain constant, although most coolant properties do not vary with temperature, and viscosity does.
3. The coolant remains in a single phase throughout the flow.
4. Heat transfer by radiation is sufficiently small so we can neglect it.
5. The flow is laminar, steady, and incompressible, ensuring stable flow conditions.
6. Thermal contact resistance at the solid–fluid interface is neglected, and perfect bonding is assumed for heat transfer.

Based on these assumptions, we developed the core equations for modelling thermal energy transfer and fluid motion.

The fluid flow has been modelled using the continuity equation, with plain water as the working coolant.

$$\nabla \cdot \vec{V} = 0 \text{ or } \frac{\partial U}{\partial X} + \frac{\partial V}{\partial Y} + \frac{\partial W}{\partial Z} = 0 \tag{1}$$

In the given equation, the flow velocities along the three spatial directions—X, Y, and Z are indicated by the variables U, V, and W in that order.

Governing Equation for Momentum

$$U\frac{\partial U}{\partial X} + V\frac{\partial U}{\partial Y} + W\frac{\partial U}{\partial Z} = -\frac{1}{\rho_{wf}}\frac{\partial P}{\partial X} + \frac{\mu_{wf}}{\rho_{wf}}\left(\frac{\partial^2 U}{\partial X^2} + \frac{\partial^2 U}{\partial Y^2} + \frac{\partial^2 U}{\partial Z^2}\right) \tag{2}$$

$$U\frac{\partial V}{\partial X} + V\frac{\partial V}{\partial Y} + w\frac{\partial V}{\partial Z} = -\frac{1}{\rho_{wf}}\frac{\partial P}{\partial X} + \frac{\mu_{f,l}}{\rho_{f}}\left(\frac{\partial^2 V}{\partial X^2} + \frac{\partial^2 V}{\partial Y^2} + \frac{\partial^2 V}{\partial Z^2}\right) \tag{3}$$

$$U\frac{\partial W}{\partial X} + v\frac{\partial W}{\partial Y} + w\frac{\partial W}{\partial Z} = -\frac{1}{\rho_{wf}}\frac{\partial P}{\partial X} + \frac{\mu_{Cf}}{\rho_{wf}}\left(\frac{\partial^2 W}{\partial X^2} + \frac{\partial^2 W}{\partial Y^2} + \frac{\partial^2 W}{\partial Z^2}\right) \tag{4}$$

In this case, the density is denoted by ρ_{wf} and dynamic viscosity is represented by where the viscosity varies according to temperature, and is expressed as

$$\mu_{wf} = \left[\left(2.414 \times 10^{-05}\right) \times \left(10\left(\frac{247.8}{T-140}\right)\right)\right] \tag{5}$$

This equation defines the temperature-dependent viscosity of μ_{wf} the working fluid. It is an empirical correlation used to evaluate the temperature dependence of viscosity and is essential for accurately predicting fluid flow and heat transfer in microchannels.

Energy equation

$$\frac{K_{wf}}{\rho_{wf}C_{pwf}}\left(\frac{\partial^2 T_{wf}}{\partial X^2} + \frac{\partial^2 T_{wf}}{\partial Y^2} + \frac{\partial^2 T_{wf}}{\partial Z^2}\right) = U\frac{\partial T_{wf}}{\partial X} + V\frac{\partial T_{wf}}{\partial Y} + W\frac{\partial T_{wf}}{\partial Z} \tag{6}$$

This equation represents the energy balance for the working-fluid domain. It accounts for both conduction (left-hand side) and convection (right-hand side) within the flowing coolant. In this case, T_{wf} refers to the working fluid temperature, C_{pwf} represents working fluid specific heat and K_{wf} denotes the working fluid thermal conductivity.

The energy equation can be applied and modified to describe heat transfer within the silicon wafer.

$$K_{sb}\left(\frac{\partial^2 T_{sb}}{\partial X^2} + \frac{\partial^2 T_{sb}}{\partial Y^2} + \frac{\partial^2 T_{sb}}{\partial Z^2}\right) = 0 \tag{7}$$

This equation describes heat conduction in the silicon substrate. Since silicon is solid and stationary, there is no convection term. Here, T_{sb} represents the substrate temperature, and K_{sb} is its thermal conductivity. This equation models heat spreading within the solid wafer, which interacts thermally with the working fluid domain.

3.2. Specified condition at the boundary

A microchannel has been set up for simulation purposes, with a fixed thermal flux of 1,000,000 W/m² applied to its base and cool water at 289 K flowing in at a steady speed. At the outlet, we maintained a neutral pressure of 0 pascal to mimic real-world fluid behavior and treated the solid-fluid interfaces as coupled walls to reflect their interplay. For the solid part, symmetric boundary conditions were applied to the side walls, and the remaining walls were set as adiabatic to minimize heat loss. We performed all simulations with

Ansys Fluent, a commercial computational fluid dynamics solver that employs the finite volume method. To maintain precision, we discretized the equations with a second-order upwind method, linked pressure and velocity using a simple algorithm, and solved the equations using the Gauss-Seidel iterative approach. To ensure the accuracy of our results, we set strict convergence criteria: residuals for the velocity and energy equations were below 10^{-6} and the residual for the continuity equation was below 10^{-4}.

3.3. Flow and thermal analysis

To analyze the flow behavior, we calculated the Reynolds number using the inlet velocity V_{in} of the employed liquid and its associated characteristics, like density (ρ_{wf}) and dynamic viscosity of the fluid (μ_{wf}). The following equation was used for this calculation**.**

Reynolds' number.

$$Re = \frac{\rho_{wf} V_{in} D_{hyd}}{\mu_{wf}} \tag{8}$$

In this context, D_{hyd} represents the hydraulic diameter for analysing the characteristics of fluid flow in channels that are not perfectly circular. The equation below defines the same:

$$D_{hyd} = \frac{4A_{ch}}{P_{ch}} \tag{9}$$

where A_{ch} is the cross-sectional area of the channel, and P_{ch} is its perimeter.

In this study, the hydraulic diameter is kept constant across all configurations. The Nusselt number is calculated using

$$Nu = \frac{hD_{hyd}}{K_{wf}} \tag{10}$$

Here, k_{wf} denotes the thermal conductivity of the coolant fluid, while h represents the average heat transfer coefficient, which is calculated using the following relation:

$$h = \frac{q_{eff}}{(T_{mean,s\text{-}1} - T_{mean,wf})} \tag{11}$$

Here, $T_{mean, s-1}$ is the average temperature occurring at the interface between the solid and liquid; it can be calculated using an area-weighted method, while $T_{mean, wf}$ is the mean temperature of the working fluid, determined using a volume-average approach.

The effective heat flux q_{eff} represents the average heat load per unit wetted interface area of the channel, obtained by redistributing the applied base heat flux over the total fluid–solid contact surface. The effective heat flux q_{eff} [58]is given by:

$$q_{eff} = \frac{qA_{hb,wall}}{A_{Intf}} \tag{12}$$

where $A_{hb, wall}$ is the constant heated base wall area, and A_{intf} is the total interface area of the channel.

To compare the thermal and hydrodynamic performance of different pin-fin microchannel designs with that of plain channels, the performance factor (PF)(1) is used:

$$PF = \frac{Nu/Nu_{pl}}{\left(\frac{\Delta P}{\Delta P_{pl}}\right)^{\frac{1}{3}}} \tag{13}$$

Here, Nu_{pl} and ΔP_{pl} represent the plain microchannel's Nusselt number and pressure drop, respectively.

The performance factor (PF) compares the thermo-hydraulic efficiency of a microchannel configuration to that of a plain channel. The numerator Nu/Nu_{pl} represents the relative heat transfer enhancement, while the denominator $\left(\frac{\Delta P}{\Delta P_{pl}}\right)^{\frac{1}{3}}$ accounts for the increase in pressure drop, with the 1/3 exponent reflecting the pumping power relationship. A PF greater than 1 implies improved overall thermal performance compared with a plain channel. Table 2 presents the thermophysical parameters of the working fluid and solid material utilised in this study.

Table 2. Thermophysical properties of the working fluid and solid material

Property	Symbol	Deionized Water (300 K)	Silicon
Density (kg/m³)	ρ	997	2330
Specific heat (J/kg·K)	Cp	4181	700
Thermal conductivity (W/m·K)	k	0.6	131
Dynamic viscosity (Pa·s)	μ	0.00114	-
Prandtl number (–)	Pr	6.99	-

3.4. Discretization error assessment

In this simulation study, we employed a hybrid meshing strategy that combined structured and unstructured regions to efficiently discretize the computational domain. To preserve uniformity and improve precision, the microchannel heat sink without a plate was designed using a homogeneous structured mesh. In contrast, plates with complex geometries were meshed using a non-uniform unstructured grid. This approach helped resolve intricate flow patterns and heat-transfer phenomena more effectively. The zigzag and triangular plate regions were refined with a finer mesh near the solid–fluid interface. This refinement was necessary to capture sharp gradients and vortex formation. Mesh-independence testing was also conducted to verify the reliability of the results.

Figure 2 illustrates the solid and fluid domains with the meshed solid–fluid interface for the zigzag and triangular configurations. To assess how mesh resolution affects the present results, a grid-independence study using three mesh densities was conducted. The sizes of 5.03 million, 7.1 million, and 13.5 million elements have been detailed in Table 3. As anticipated, finer meshes reduced numerical errors, but this came at the cost of significantly increased computational time. After analyzing the results, we observed that the pressure drops and Nusselt number differed by only 0.79% and 0.11%, respectively, between the 7.1-million-element and 13.5-million-element grids. These minimal variations suggest that further mesh refinement yields negligible benefits. Based on this, we chose the 5.03-million-element grid for the remaining simulations, as it strikes an appropriate balance between numerical accuracy and simulation speed.

Table 3. Comparison of different mesh densities

Element Quantity	Nu	e%	Drop in Pressure (Pa)	e%
5032165	10.34	2.17391	8486.952	1.163752
7165301	10.12	0.79681	8586.882	0.117135
13525325	10.04	-	8596.952	-

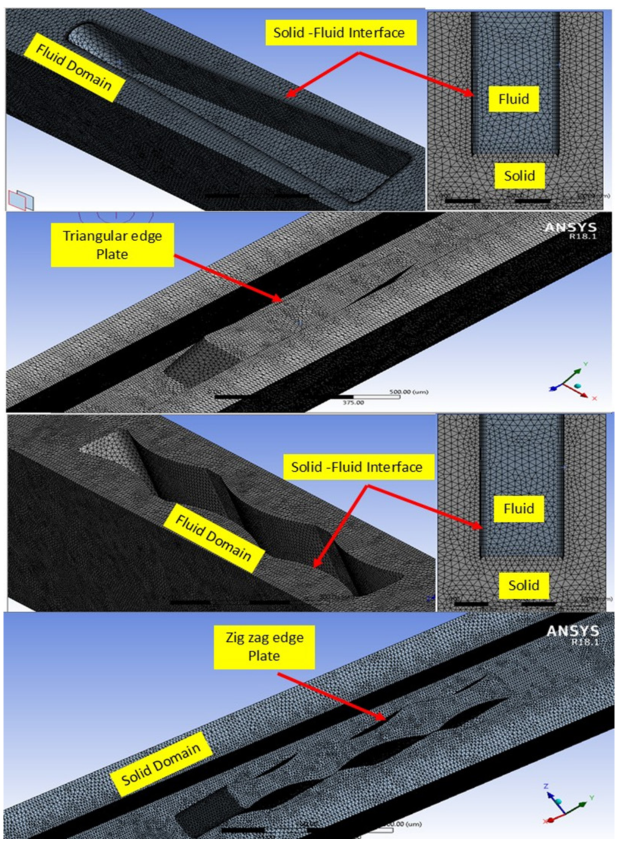

Figure 2. Solid and fluid domains with meshed solid–fluid interface for **(a)** zigzag edge plate microchannel and **(b)** triangular edge plate microchannel

3.5. Comparison between numerical and reference results

The numerical results were corroborated by the experimental data of Qu et al. (2) to ensure model accuracy. Our analysis focuses on a representative microchannel heat sink unit from their study. The comparison illustrated in Figure 3 shows alignment between simulation results and experimental measurements of pressure loss and the thermal profile along the microchannel, confirming their agreement. Figure 3(a) shows a detailed comparison of pressure loss in the microchannel across a range of Reynolds numbers and at heat fluxes of 100 and 200 W/cm². Meanwhile, Figure 3(b)depicts the temperature distribution at four distinct locations within the channel at a heat flux of 100 W/cm².The numerical results show excellent agreement with the experimental data, with discrepancies typically within 3-6%(3), which falls well inside the acceptable range reported in literature for the examination of heat transport and fluid dynamics.

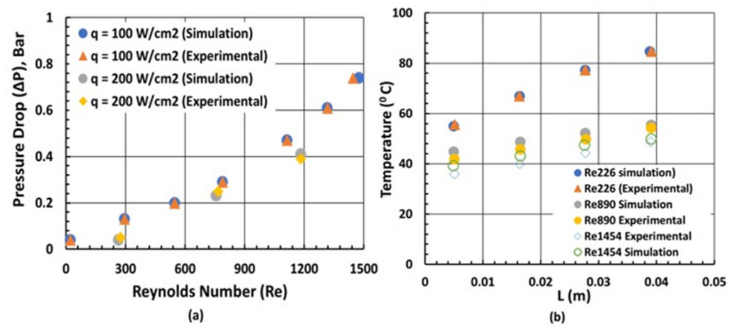

Figure 3. Numerical vs. experimental **(a)** Pressure variation and **(b)** temperature distribution across four positions in the channel (L_1 = 0.01 m, L_2 = 0.02 m, L_3 = 0.03 m, L_4 = 0.04 m from inlet) under a heat flux of 100 W/cm², comparing simulation and experimental results

4. Findings and analysis

4.1. Thermal–hydraulic performance evaluation of different MCHS configurations

Figure 4 examines the performance of three microchannel heat sink designs: plain channels, triangular edge plates, and zigzag edge plates. The comparison includes the maximum base temperature, thermal resistance, Nusselt number, heat transfer coefficient, pressure drop, and thermal performance factor. The plain channel, with streamlined laminar flow, as shown in Figure 6, exhibits the lowest pressure drop but restricted heat transfers due to an undisturbed thermal boundary layer, resulting in the lowest Nusselt number. The triangular design introduces flow asymmetry, leading to intensified secondary circulation and mixing, thereby balancing thermal and hydraulic performance while improving Nusselt numbers. The zigzag design, despite incurring the highest pressure drop due to sharp flow changes, offers the best thermal performance through vigorous mixing and disturbance of the boundary layer, leading to the maximum Nusselt number and heat transfer coefficient.

The velocity and streamline contours presented in Figures 5 and 6 together illustrate the distinct flow physics of the three microchannel configurations. In the plain channel, the velocity field remains nearly parallel, and the streamlines are smooth with little disturbance. This results in a continuously thickening boundary layer, reduced wall-temperature gradients, and limited heat transfer. In contrast, the triangular edge plates induce local flow separation and reattachment which periodically thin the boundary layer and enhance heat transfer, as observed in both velocity and streamline contours; however, this effect remains spatially confined. The zigzag-edge plates exhibit the most significant improvement, with their wavy geometry repeatedly disrupting and reinitiating the boundary layer. The velocity contours in Figure 5 reveal alternating streaks of high and low velocity whereas the streamline contours in Figure 6 indicate repeated vortex formation. These vortices enhance cross-stream mixing, maintain high wall shear, and sustain steep temperature gradients along the channel walls. Thus, the zigzag configuration achieves optimal values of the heat transfer coefficient and the Nusselt number. Although accompanied by an increased pressure drop, the design's overall balance confirms its superior thermal performance compared with the other designs.

Collectively, Figures 5 and 6 highlight the enhanced flow and thermal behaviors of the triangular and zigzag designs relative to the plain channel. In the triangular configuration, sharp edges generate recirculation zones immediately downstream of the plate, where the local velocity drops below 0.5 m/s, compared with the core flow velocity of about 3.5–4.0 m/s. The size of these recirculation zones extends to roughly 0.5–0.7 times the channel height, which promotes moderate mixing and a corresponding increase in pressure loss. In contrast, the zigzag design induces stronger and more complex flow dynamics. The sudden contractions and expansions accelerate the fluid locally to 3.8–4.0 m/s, while vortex structures form in the cavities where velocities drop below 0.3 m/s. These vortices occupy nearly the entire channel height and extend longitudinally about 1.0–1.2 times that height, as shown in Figure 6. The strong velocity gradients between accelerated jet-like regions and low-velocity recirculation zones cause significant boundary-layer disruption, leading to enhanced heat-transfer performance, but requiring greater pumping power.

The outcomes of this study have important implications for thermal management system design. The plain microchannel configuration is advantageous in applications where minimal pumping power is prioritized, whereas the triangular geometry offers a compromise between enhanced heat transfer and moderate pressure loss. The zigzag configuration, despite its higher hydraulic penalty, demonstrates superior heat dissipation capacity and is therefore most suitable for high heat flux applications. Collectively, these insights establish a direct link between flow physics and application-specific requirements, offering a rational basis for the selection and optimization of microchannel geometries in advanced cooling systems.

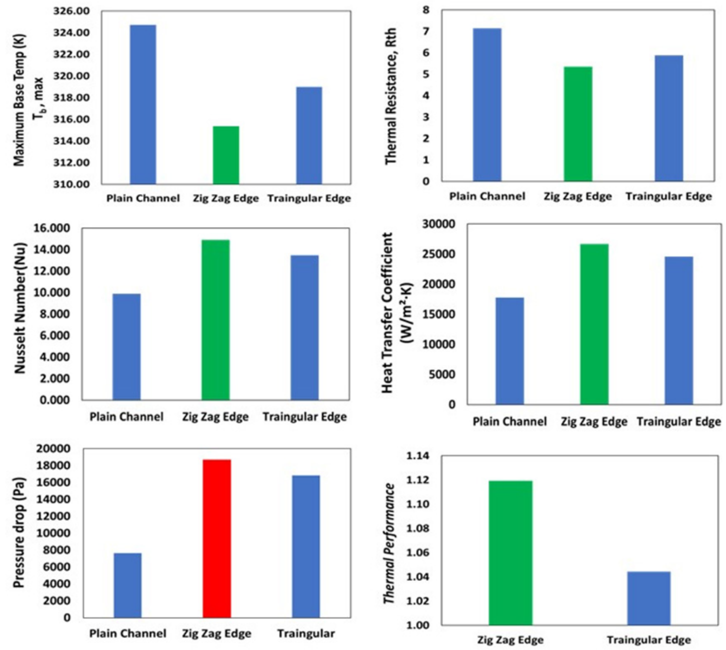

Figure 4. Thermo-hydraulic performance of plain, triangular, and zigzag microchannel heat sinks at Re = 250

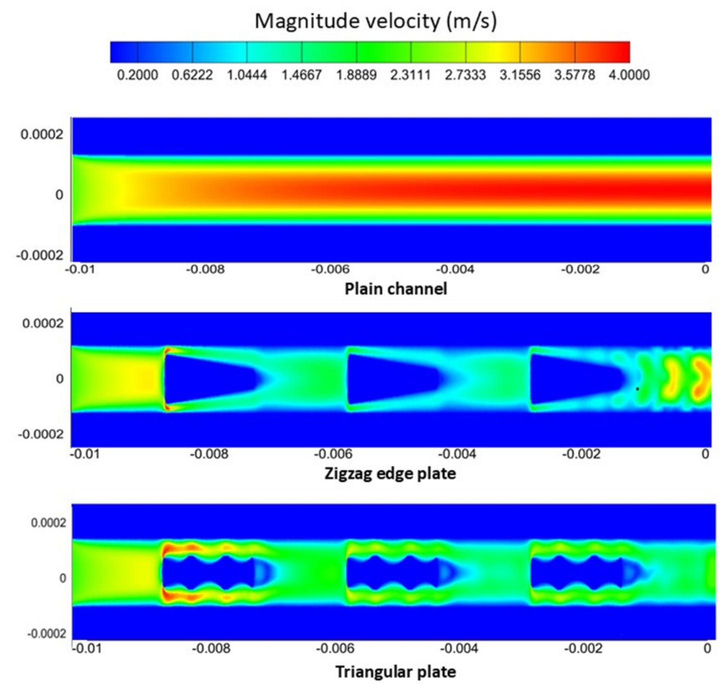

Figure 5. Velocity contours in microchannel heat sinks at Re = 250, demonstrating the role of geometry in flow behavior, acceleration, and overall fluid dynamics

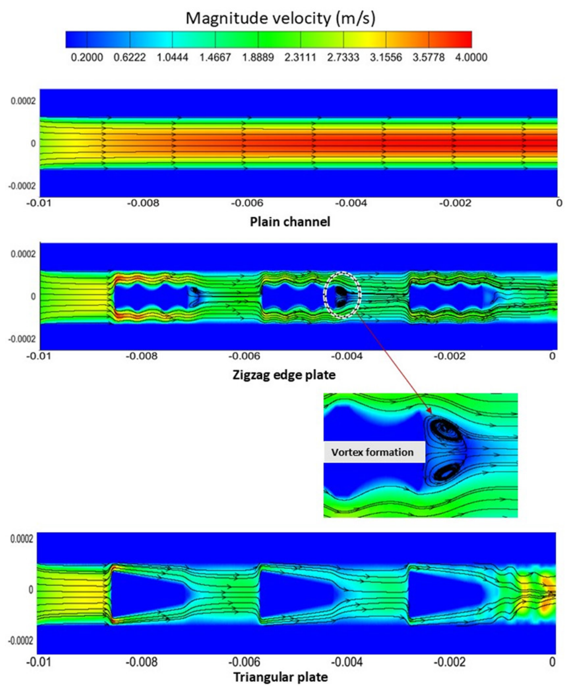

Figure 6. Streamline contours in microchannel heat sinks at Re = 250, showing the influence of geometry on flow behaviour and distribution

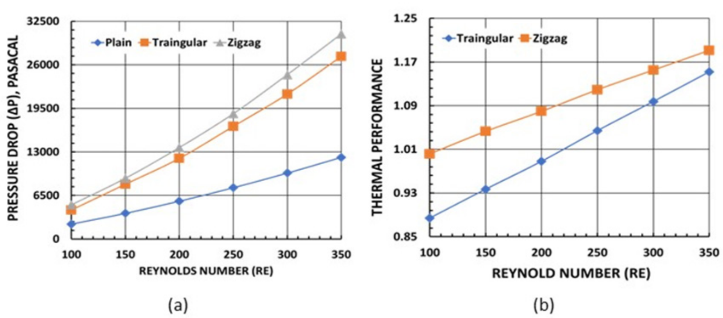

Figure 7. Pressure drops and thermal performance vs. Reynolds number for different microchannel configurations

4.2. Zigzag edge plate microchannel: enhanced cooling with higher pressure loss

Figure 7 compares the thermal performance factor (TPF), and the pressure drop for plain, triangular, and zigzag microchannels. The results are presented with different Reynolds numbers. The plots highlight the thermo-hydraulic trade-offs of each design. In Figure 7(a), pressure loss increases with Reynolds number for all designs. The plain microchannel exhibits the lowest pressure drop. The triangular design exhibits a moderate rise due to vortex formation. The zigzag configuration exhibits the greatest loss which results from strong secondary flows and sharp directional changes. Figure 7(b) shows that the zigzag design achieves the highest TPF, reaching 1.20 at Re = 350. This is due to enhanced mixing and repeated boundary layer disruption. Although it requires higher pumping power, the zigzag design remains the most efficient for cooling, particularly at higher Reynolds numbers.

Compared with the triangular design, the zigzag design thermally outperforms it by 11.77% at Re=100, 10.19% at Re=150, 8.49% at Re=200, 6.70% at Re=250, 4.97% at Re=300, and 3.29% at Re=350 the improvement decreases as the flow rate increases. At higher Reynolds numbers, the thermal boundary layer becomes thinner. Fluid mixing also increases at higher flow rates. Therefore, the additional benefit provided by vortices generated at the zigzag edges is reduced. The zigzag design still performs better than the other geometries. However, its advantage diminishes as the Reynolds number increases.

The results in Figure 7(b) show that the zigzag edge configuration achieves the highest TPF (1.20 at Re = 350). This advantage is offset by higher pressure losses. The plain channel remains hydraulically efficient but is thermally weak. The triangular channel provides an intermediate balance. Similar thermo-hydraulic trade-offs have been reported in wavy and ribbed microchannels [11, 12, 21]. In those cases, enhanced mixing improved heat transfer but also increased pressure loss.

The zigzag design outperforms the triangular design by 11.77% at Re = 100. This advantage decreases to 3.29% at Re = 350. The added benefit of vortices decreases at higher flow rates, where natural mixing is already strong. This trend is consistent with earlier findings in wavy-edge and ribbed channels [28, 31, 37]. Overall, the present study shows that simple plate-edge modifications can deliver significant thermal enhancement. They also provide a practical alternative to more complex channel inserts. These findings highlight the practical value of edge-modified microchannels for compact cooling solutions. The zigzag design, with a TPF of 1.20 at Re = 350, achieves thermal performance up to 11.77% higher than that of the triangular geometry, making it suitable for use in high-heat-flux devices such as microprocessors and laser diodes. The triangular configuration offers a balanced option in which moderate enhancement is required and pumping penalties are lower, while the plain channel remains efficient in low-power applications. Thus, simple plate-edge modifications present a cost-effective and scalable alternative to complex inserts for thermal management.

4.3. Triangular plate: moderate heat transfer efficiency with balanced pressure drop

The triangular plate-integrated microchannel improves thermal performance over the plain channel by periodically disrupting the boundary layer. The inclined surfaces of the triangular features generate secondary flows that enhance fluid mixing and convective heat transport. As shown in Figures 8(a) and 8(b), the triangular configuration consistently outperforms the plain channel across the entire Reynolds number range. At Re = 100, the triangular plate achieves a heat transfer coefficient of 15,647.76 W/m² K, compared with 12,401.62 W/m²K for the plain channel, corresponding to a 20.75% enhancement. Similarly, at Re = 350, the triangular channel reaches 29,245.46 W/m²K, representing a 32.52% improvement over the plain value of 19,733.64 W/m²K.

Although the triangular geometry provides substantial improvement, its performance remains consistently below that of the zigzag configuration. For instance, at Re = 200, the triangular plate records 21,800.53 W/m²K, while the zigzag achieves 24,120.47 W/m²K, yielding an additional advantage of 10.64%. Across the entire range, zigzag enhancement varies between 32.01% and 38.21%, compared to 20.75%–32.52% for the triangular plate. However, as shown by the pressure-drop curve in Figure 7(a), this thermal gain comes with a moderate increase in flow resistance higher than that of the plain design but significantly lower than that of the zigzag plate. Thus, while the triangular design does not induce as strong a mixing effect as the zigzag geometry, it offers a favorable compromise between thermal enhancement and hydraulic penalty. Its ability to achieve 29–32% heat transfer improvement at high Reynolds numbers while requiring comparatively lower pumping power makes it a practical and efficient choice for compact cooling applications.

The present findings align well with earlier reports on wavy and ribbed microchannels [11,12,21,28,31,37], where geometric modifications enhanced fluid mixing and heat transfer but at the cost of higher pressure drop. Consistent with those studies, the triangular plate exhibits balanced performance, achieving a 20–32% increase in the heat transfer coefficient with only a moderate hydraulic penalty. While zigzag geometries exhibit stronger augmentation (32–38%), the triangular plate offers a more practical trade-off between thermal efficiency and pumping power, positioning it as an effective alternative to more complex channel inserts for compact cooling applications.

The results demonstrate that triangular plate-integrated microchannels provide a practical balance between enhanced cooling and manageable pumping requirements. They deliver heat transfer improvements ranging from 20.75% at Re = 100 to 32.52% at Re = 350, yielding significant thermal gains over plain channels while avoiding the excessive pressure penalties associated with zigzag designs. This makes them well-suited for compact electronic and energy systems where reliability, efficiency, and manufacturability are critical. This study demonstrates that simple plate-edge integration can achieve substantial thermal enhancement, providing a cost-effective and scalable alternative to more intricate microchannel modifications.

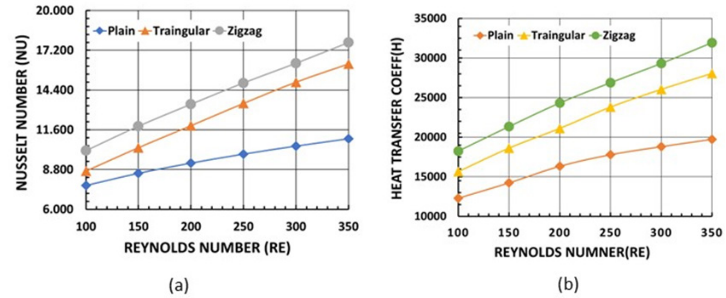

Figure 8. Comparing Heat Transfer capability: **(a)** NusseltaNusseltnd **(b)**Heat Transfer Coefficient Across Plain, Triangular, and Zigzag Configurations with Increasing Reynolds Number

4.4. Thermal resistance and base temperature reduction in modified microchannel geometries

The base wall temperature contours, as illustrated in Figure 9, demonstrate the impact of geometry on cooling effectiveness. The plain channel shows a large red zone near the outlet, indicating poor heat removal. In contrast, the triangular and zigzag plates display cooler regions(green–blue), confirming enhanced wall cooling and more uniform heat dissipation.

As depicted in Figure 10(a), the maximum base temperature decreases consistently as the Reynolds number increases across all configurations. Compared with the plain channel, the zigzag design achieves larger reductions of 7.51–9.43 K, whereas the triangular plate shows smaller reductions of 2.19–6.91 K. This indicates stronger mixing and improved wall interaction in the zigzag configuration, particularly at lower to moderate Reynolds numbers.

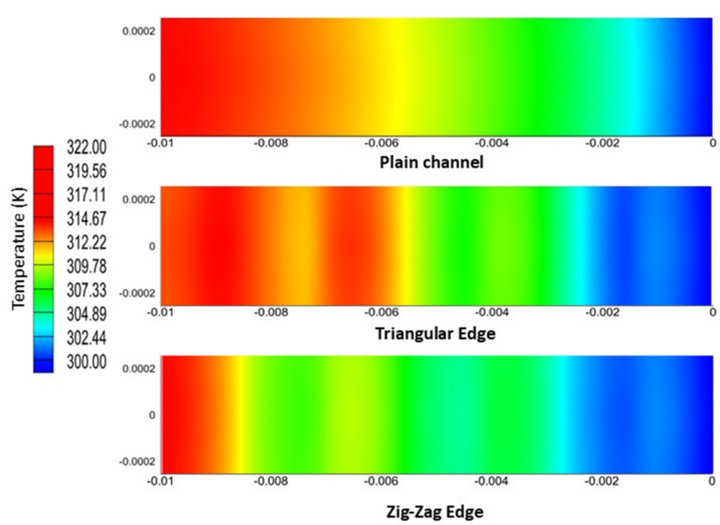

Figure 9. Temperature contours of the base wall for all tested geometries at Re = 300

Figure 10(b) illustrates that higher Reynolds numbers correspond to reduced thermal resistance. Within Re = 100–350, the thermal resistance of the zigzag plate decreases from 8.4 to 3.8 K/W, while that of the triangular plate decreases from 9.5 to 5.0 K/W. Compared to the plain channel, the zigzag edge plate achieves a 41.1% reduction, and the triangular plate achieves 21.41% reduction. The zigzag geometry creates stronger vortices yielding improved wall cooling and reduced resistance, whereas the triangular design forms stable recirculation zones and produces a smaller reduction. Overall, the zigzag configuration is more effective in reducing maximum wall temperature, while the triangular configuration ensures a significant decrease in thermal resistance, especially at higher Reynolds numbers.

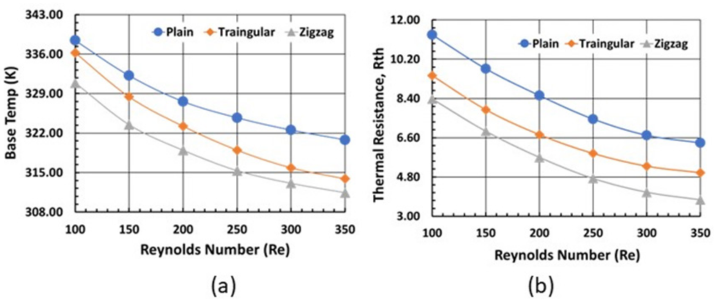

Figure 10. Variation of **(a)** maximum base temperature and **(b)** thermal resistance with Reynolds number (Re = 100–350)

5. Conclusion

Effective thermal management is essential for the performance and endurance of high-power-density electronic equipment. This study explored a unique technique to improve microchannel heat sink (MCHS)performance by integrating internal plate geometries—specifically triangular and zigzag edge-plates—within the channel structure. The goal was to improve heat dissipation in compact processors like the Intel Core i5-7600K.

Three MCHS designs—plain rectangular, triangular edge-plate, and zigzag edge-plate—were numerically analyzed for varying Reynolds numbers to evaluate the Nusselt number, heat transfer coefficient, pressure drop, and thermal performance factor.

- The plain channel design provided the lowest pressure drop but exhibited limited thermal performance due to minimal flow disturbance.
- The triangular edge-plate configuration enhanced secondary flow, achieving a moderate thermal performance factor of 1.15.
- The zigzag edge-plate design delivered superior results, achieving a 38.21% increase in the heat transport coefficient compared to the plain design and a maximum thermal performance factor of 1.20. Additionally, it outperformed the triangular configuration by 11.77% at low Reynolds numbers, demonstrating its effectiveness in enhancing thermal performance through improved fluid mixing and boundary layer disruption.
- Despite an increased pressure drop, the zigzag configuration consistently outperformed other configurations across all flow regimes.

This study introduces an effective geometric enhancement strategy for MCHSs, offering new insights into compact high-efficiency thermal solutions for next-generation electronic cooling systems.

6. Future scope

This study shows that triangular and zigzag edge-plate geometries can enhance the thermal performance of microchannel heat sinks. However, further work is required to expand the scope. Experimental validation is needed to confirm the numerical results and ensure practical reliability. Other geometries, such as wavy ribs, pin-fins, or hybrid structures, may provide better performance with controlled pressure drops. The use of advanced materials, surface coatings, or nanostructured walls could also enhance heat transfer. Similarly, nano fluids, dielectric liquids, or phase-change fluids may offer additional benefits. Studies under transient and non-uniform heat loads are necessary to represent actual processor operating conditions. Future work can also combine these designs with hybrid cooling methods such as jet impingement or two-phase flow. Finally, the approach should be extended to multi-chip modules, GPUs, and server-grade processors to test scalability for next-generation systems.

Author contributions statement

Anas Khan: Investigation, Methodology, Software, Data curation, Formal analysis, Visualization, Writing – original draft. Mahmood Alam: Conceptualization, Supervision, Methodology, Validation, Formal analysis, Writing – review & editing, Project administration. Mohammad Nawaz Khan: Validation, Investigation, Writing – review & editing. Mohd. Anas: Software, Data curation, Visualization, Writing – review & editing. Abhishek Dwivedi: Formal analysis, Validation, Writing – review & editing.

Declaration of interests

The authors declare that they have no known competing financial interests or personal relationships that could have appeared to influence the work reported in this paper.

Data availability

The data that support the findings of this study are available from the corresponding author upon reasonable request.

Declaration of generative AI and AI-assisted technologies in the writing process

The authors did not use generative AI or AI-assisted technologies in the writing process of this manuscript.

Nomenclature

Symbols

A_{ch}	Channel Area
$A_{hb, wall}$	Area of Heated Base Wall
A_{Intf}	Total Interface Area
C_{pwf}	Specific Heat of Working Fluid
D_{hyd}	Hydraulic Diameter
h	Heat Transfer Coefficient
H_{ch}	Height of Channel
H_{sb}	Height of Substrate
K_{sb}	Thermal Conductivity of Silicon Substrate
K_{wf}	Thermal Conductivity of Working Fluid
Nu	Nusselt Number
P_{ch}	Channel Perimeter
q_{eff}	Effective Heat Flux
Re	Reynolds Number
$T_{mean, s-l}$	Mean Temperature at Solid–Liquid Interface
$T_{mean, wf}$	Mean Temperature of Working Fluid
T_{sb}	Temperature of Silicon Substrate
T_{wf}	Temperature of Working Fluid
W_{ch}	Width of Channel
W_{sb}	Width of Substrate

Greek Symbols

μ_{wf}	Dynamic Viscosity of Working Fluid
μ_{Cf}	Temperature-Dependent Dynamic Viscosity
ρ_{wf}	Density of Working Fluid
α	Non-dimensional perforation diameter of the pin fin

Abbreviation

CHF	Critical Heat Flux
DP-MCHS-PS	Dual-Passage Microchannel Heat Sink with Pin Structures
FVM	Finite Volume Method
G/D	Gap-to-Diameter Ratio
HTC	Heat Transfer Coefficient
MCHS	Microchannel Heat Sink
MC-SOCRR	Microchannel with Secondary Oblique Cross Ribs & Ribs
NSGA	Non-dominated Sorting Genetic Algorithm
PEC	Performance Evaluation Criterion
PF	Performance Factor
PPF	Piranha Pin Fin
TPF	Thermal Performance Factor
VLSI	Very Large-Scale Integration
W/cm^2	Watts per Square Centimeter
GA	Genetic algorithm
BPNN	Back propagation neural network

References

[1] M. Z. M. Hanafi, F. S. Ismail, and R. Rosli, "Radial plate fins heat sink model design and optimization," in 2015 10th Asian Control Conference: Emerging Control Techniques for a Sustainable World, ASCC 2015, p. 5, 2015. https://doi.org/10.1109/ASCC.2015.7244448

[2] V. Lakshminarayanan and N. Sriraam, "The effect of temperature on the reliability of electronic components," in IEEE CONECCT 2014 - 2014 IEEE International Conference on Electronics, Computing and Communication Technologies, pp. 1–6, 2014. https://doi.org/10.1109/CONECCT.2014.6740182.

[3] M. S. M. Saleh, Y. Belloufi, Y. Boutera, A. J. Chamkha, A. Sahraoui, and Q. Hroub, "A new design for a heat sink within a convex-parabolic microchannel filled with hybrid nanofluid for cooling Core I7 CPU," J. Therm. Anal. Calorim., vol. 148, no. 20, pp. 11315–11324, 2023. https://doi.org/10.1007/s10973-023-12404-w.

[4] D. B. Tuckerman and R. F. W. Pease, "High-Performance Heat Sinking for VLSI," IEEE Electron Device Lett., vol. EDL-2, no. 5, pp. 126–129, 1981. https://doi.org/10.1109/EDL.1981.25367.

[5] D. Cooke and S. G. Kandlikar, "Pool boiling heat transfer and bubble dynamics over plain and enhanced microchannels," J. Heat Transfer, vol. 133, no. 5, 2011. https://doi.org/10.1115/1.4003046.

[6] R. Kaniowski, R. Pastuszko, and L. Nowakowski, "Effect of geometrical parameters of open microchannel surfaces on pool boiling heat transfer," EPJ Web Conf., vol. 143, pp. 0–4, 2017. https://doi.org/10.1051/epjconf/201714302049.

[7] A. Jaikumar and S. G. Kandlikar, "Ultra-high pool boiling performance and effect of channel width with selectively coated open microchannels," Int. J. Heat Mass Transf., vol. 95, pp. 795–805, 2016. https://doi.org/10.1016/j.ijheatmasstransfer.2015.12.061.

[8] M. H. R. Yasin Khan, Md Tanbir Sarowar, Mahir Mobarrat, "Performance Comparison of a Microchannel Heat Sink Using Different Nano-Liquid Metal Fluid Coolant: A Numerical Study," J. Therm. Sci. Eng. Appl., vol. 14(9): 091, 2022. https://doi.org/https://doi.org/10.1115/1.4054007.

[9] B. Jalili, N. Aghaee, P. Jalili, and D. Domiri Ganji, "Novel usage of the curved rectangular fin on the heat transfer of a double-pipe heat exchanger with a nanofluid," Case Stud. Therm. Eng., vol. 35, no. April, p. 102086, 2022. https://doi.org/10.1016/j.csite.2022.102086.

[10] C. Li, H. Roshani, M. Jalili, M. H. Mohamed, P. Jalili, B. Jalili, I. Ahmad, and Q. M. Al-Mdallal, "Influence of hybrid nanofluids on entropy dynamics and transient thermal behavior in

a finned enclosure with cylindrical obstruction," Case Stud. Therm. Eng., vol. 72, no. January, p. 106339, 2025. https://doi.org/10.1016/j.csite.2025.106339.

[11] A. Belhadj, R. Bouchenafa, and R. Saim, "Numerical investigation of forced convection of nanofluid in microchannel heat sinks," J. Therm. Eng., vol. 4, no. 5, pp. 2263–2273, 2018. https://doi.org/10.18186/thermal.438480.

[12] H. A. Mohammed, P. Gunnasegaran, and N. H. Shuaib, "Influence of channel shape on the thermal and hydraulic performance of microchannel heat sink," Int. Commun. Heat Mass Transf., vol. 38, no. 4, pp. 474–480, 2011. https://doi.org/10.1016/j.icheatmasstransfer.2010.12.031.

[13] A. Sharma and M. K. Khan, "Heat transfer and flow characteristics of varying curvature wavy microchannels," Int. J. Therm. Sci., vol. 185, no. September 2022, p. 108096, 2023. https://doi.org/10.1016/j.ijthermalsci.2022.108096.

[14] A. Eltaweel and I. Hassan, "A Multivariable Numerical Investigation of Wavy-Based Microchannel Heat Sink Geometry Toward Optimal Thermal Performance," J. Therm. Sci. Eng. Appl., vol. 16, no. 11, Nov. 2024. https://doi.org/10.1115/1.4066263.

[15] M. Zunaid, A. Jindal, D. Gakhar, and A. Sinha, "Numerical study of pressure drop and heat transfer in a straight rectangular and semi cylindrical projections microchannel heat sink," J. Therm. Eng., vol. 3, no. 5, pp. 1453–1465, 2017. https://doi.org/10.18186/journal-of-thermal-engineering.338903.

[16] B. Jalili and P. Jalili, "Numerical analysis of airflow turbulence intensity effect on liquid jet trajectory and breakup in two-phase cross flow," Alexandria Eng. J., vol. 68, pp. 577–585, 2023. https://doi.org/10.1016/j.aej.2023.01.059.

[17] D. Salehipour, B. Jalili, and P. Jalili, "Effect of humidification of combustion products in the boiler economizer with spiral geometry," Results Eng., vol. 21, no. July 2023, p. 101906, 2024. https://doi.org/10.1016/j.rineng.2024.101906.

[18] P. Jalili and B. Jalili, "Computational fluid dynamics simulation of enhanced heat transfer in ground-air heat exchangers using turbulators in PVC pipe systems," Case Stud. Therm. Eng., vol. 68, no. November 2024, p. 105949, 2025. https://doi.org/10.1016/j.csite.2025.105949.

[19] L. Chai, G. Xia, M. Zhou, J. Li, and J. Qi, "Optimum thermal design of interrupted microchannel heat sink with rectangular ribs in the transverse microchambers," Appl. Therm. Eng., vol. 51, no. 1–2, pp. 880–889, 2013. https://doi.org/10.1016/j.applthermaleng.2012.10.037.

[20] I. A. Ghani, N. A. C. Sidik, R. Mamat, G. Najafi, T. L. Ken, Y. Asako, and W. M. A. A. Japar, "Heat transfer enhancement in microchannel heat sink using hybrid technique of ribs and secondary channels," Int. J. Heat Mass Transf., vol. 114, pp. 640–655, 2017. https://doi.org/10.1016/j.ijheatmasstransfer.2017.06.103.

[21] G. Wang, N. Qian, and G. Ding, "Heat transfer enhancement in microchannel heat sink with bidirectional rib," Int. J. Heat Mass Transf., vol. 136, pp. 597–609, 2019. https://doi.org/10.1016/j.ijheatmasstransfer.2019.02.018.

[22] V. P. Gaikwad, S. S. Mohite, S. S. Shinde, and M. L. Dherange, "Enhancement in Thermo-Hydraulic Performance of Microchannel Heat Sink With Secondary Flows of Leaf Venation Pattern," J. Therm. Eng., vol. 6, no. 5, pp. 677–696, 2020. https://doi.org/10.18186/thermal.790258.

[23] Q. Zhu, Z. Wang, J. Zeng, X. Wen, H. Deng, W. He, and T. Zhao, "Numerical study on flow and heat transfer in a novel symmetric sinusoidal wavy microchannel heat sink with rectangular rib prisms," Int. J. Therm. Sci., vol. 197, no. September 2023, p. 108807, 2024. https://doi.org/10.1016/j.ijthermalsci.2023.108807.

[24] L. Du, W. Hu, N. Deng, Z. Zhang, and H. Wang, "Computational analysis of heat transfer and fluid flow characteristics in a diamond microchannel heat sink with orthogonal ribs," Case Stud. Therm. Eng., vol. 67, no. February, p. 105850, 2025. https://doi.org/10.1016/j.csite.2025.105850.

[25] A. Gönül and A. B. Okbaz, "Enhanced performance of a microchannel with rectangular vortex generators," J. Therm. Eng., vol. 9, no. 2, pp. 260–278, 2023. https://doi.org/10.18186/thermal.1272395.

[26] N. Ali, I. Haque, T. Alam, T. U. Siddiqui, M. A. Ansari, J. Yadav, S. Srivastava, E. Cuce, I. Ashraf, and D. Dobrotă, "Numerical investigation on heat transfer and flow mechanism in microchannel heat sink having V shape ribs," Case Stud. Therm. Eng., vol. 65, no. October 2024, p. 105684, Jan. 2025. https://doi.org/10.1016/j.csite.2024.105684.

[27] F. Alnaimat, A. Rahhal, B. Mathew, and A. Berrouk, "Fluid flow and heat transfer investigation of microchannel heat sink with sidewall triangle ribs," Int. J. Thermofluids, vol. 26, no. February, p. 101141, 2025. https://doi.org/10.1016/j.ijft.2025.101141.

[28] N. R. Kuppusamy, H. A. Mohammed, and C. W. Lim, "Numerical investigation of trapezoidal grooved microchannel heat sink using nanofluids," Thermochim. Acta, vol. 573, pp. 39–56, 2013. https://doi.org/10.1016/j.tca.2013.09.011.

[29] H. E. Ahmed and M. I. Ahmed, "Optimum thermal design of triangular, trapezoidal and rectangular grooved microchannel heat sinks," Int. Commun. Heat Mass Transf., vol. 66, pp. 47–57, 2015. https://doi.org/10.1016/j.icheatmasstransfer.2015.05.009.

[30] P. Jalili, K. Kazerani, B. Jalili, and D. D. Ganji, "Investigation of thermal analysis and pressure drop in non-continuous helical baffle with different helix angles and hybrid nano-particles," Case Stud. Therm. Eng., vol. 36, no. June, p. 102209, 2022. https://doi.org/10.1016/j.csite.2022.102209.

[31] S. L. Sun, D. Liu, Y. Z. Wang, Y. L. Qi, and H. B. Kim, "Convective heat transfer and entropy generation evaluation in the Taylor–Couette flow under the magnetic field," Int. J. Mech. Sci., vol. 252, no. March, p. 108373, 2023. https://doi.org/10.1016/j.ijmecsci.2023.108373.

[32] Q. Zhu, H. Xia, J. Chen, X. Zhang, K. Chang, H. Zhang, H. Wang, J. Wan, and Y. Jin, "Fluid flow and heat transfer characteristics of microchannel heat sinks with different groove shapes," Int. J. Therm. Sci., vol. 161, no. October, p. 106721, 2021. https://doi.org/10.1016/j.ijthermalsci.2020.106721.

[33] V. T. M. Pankaj Kumar, "An Optimization of Grooves Structure for Thermal Performance Enhancement in Microchannel Heat Sink," Heat Transf. Eng., vol. 45, no. 17–18, 2023.

[34] Q. Wang, J. Tao, Z. Cui, T. Zhang, and G. Chen, "Numerical simulation of fluid and heat transfer characteristics of microchannel heat sink with fan-shaped grooves and triangular truncated ribs," Int. Commun. Heat Mass Transf., vol. 155, no. May, p. 107580, 2024. https://doi.org/10.1016/j.icheatmasstransfer.2024.107580.

[35] L. Liu, L. Zhang, X. Zhang, H. Xu, H. Zhang, S. Zhou, and Y. Cao, "Thermohydraulic performance of the microchannel heat sinks with three types of double-layered staggered grooves," Int. J. Therm. Sci., vol. 201, no. February, p. 109032, 2024. https://doi.org/10.1016/j.ijthermalsci.2024.109032.

[36] B. Li, Y. Cui, G. Li, and H. Jiang, "Numerical analysis on thermal-hydraulic performance of optimized microchannel heat sink with slant ribs and quatrefoil rib-elliptical groove complex structures," Appl. Therm. Eng., vol. 240, no. November 2023, p. 122165, 2024. https://doi.org/10.1016/j.applthermaleng.2023.122165.

[37] Y. Li, C. Zhu, G. Xia, and B. Yang, "Experimental investigation on the phase change liquid cooling characteristics in the offset grooved microchannel heat sink," Appl. Therm. Eng., vol. 269, no. PA, p. 126032, 2025. https://doi.org/10.1016/j.applthermaleng.2025.126032.

[38] V. P. Gaikwad and S. S. Mohite, "Performance analysis of microchannel heat sink with flow disrupting pins," J. Therm. Eng., vol. 8, no. 3, pp. 402–425, 2022. https://doi.org/10.18186/thermal.1117391.

[39] M. Liu, D. Liu, S. Xu, and Y. Chen, "Experimental study on liquid flow and heat transfer in micro square pin fin heat sink," Int. J. Heat Mass Transf., vol. 54, no. 25–26, pp. 5602–5611, 2011. https://doi.org/10.1016/j.ijheatmasstransfer.2011.07.013

[40] M. N. S. Jani and N. H. Saeid, "Thermal stress analysis in pin fin microchannel heat sink," J. Therm. Eng., vol. 10, no. 2, pp. 273–285, 2023. https://doi.org/10.18186/THERMAL.1448547.

[41] O. O. Adewumi, T. Bello-Ochende, and J. P. Meyer, "Constructal design of combined microchannel and micro pin fins for electronic cooling," Int. J. Heat Mass Transf., vol. 66, pp. 315–323, 2013. https://doi.org/10.1016/j.ijheatmasstransfer.2013.07.039.

[42] T. Izci, M. Koz, and A. Koşar, "The effect of micro pin-fin shape on thermal and hydraulic performance of micro pin-fin heat sinks," Heat Transf. Eng., vol. 36, no. 17, pp. 1447–1457, 2015. https://doi.org/10.1080/01457632.2015.1010921.

[43] X. Yu, C. Woodcock, Y. Wang, J. Plawsky, and Y. Peles, "A comparative study of flow boiling in a microchannel with piranha pin fins," J. Heat Transfer, vol. 138, no. 11, pp. 1–12, 2016. https://doi.org/10.1115/1.4033743.

[44] Y. Jia, G. Xia, Y. Li, D. Ma, and B. Cai, "Heat transfer and fluid flow characteristics of combined microchannel with cone-shaped micro pin fins," Int. Commun. Heat Mass Transf., vol. 92, pp. 78–89, 2018. https://doi.org/10.1016/j.icheatmasstransfer.2017.11.004.

[45] J. Xie, H. Yan, B. Sundén, and G. Xie, "The influences of sidewall proximity on flow and thermal performance of a microchannel with large-row pin-fins," Int. J. Therm. Sci., vol. 140, no. November 2018, pp. 8–19, 2019. https://doi.org/10.1016/j.ijthermalsci.2019.02.031.

[46] S. K. Mohammad Owais Qidwai, Irfan Anjum Badruddin, "Heat transfer enhancement in multijet micropin fin heat sink," Numer. Heat Transf. Part A Appl. An Int. J. Comput. Methodol., vol. Volume 86, no. 9, 2025. https://doi.org/10.1080/10407782.2023.2294349

[47] S. Ali, S. Alam, and M. N. Khan, "Effect of cylindrical ribs arrangement in the cavity region of the microchannel heatsink with a fan-shaped cavity," Proc. Inst. Mech. Eng. Part E J. Process Mech. Eng., Feb. 2024. https://doi.org/10.1177/09544089241231481.

[48] M. H. Mukhtar, M. N. Khan, B. P. Singh, and M. A. Ansari, "Effect of variation in heights of cylindrical pinfins on the thermo-hydraulic performance of an open-microchannel heat sink," Numer. Heat Transf. Part B Fundam., vol. 87, no. 1, Dec. 2026. https://doi.org/10.1080/10407790.2024.2341326

[49] M. O. Q. Mohammad Nawaz Khan, Munawwar Nawab Karimia, "Effect of circular perforated pin fin on heat transfer and fluid flow characteristics of rectangular microchannel heat sink," Numer. Heat Transf. Part A Appl. An Int. J. Comput. Methodol., vol. Volume 83, no. 6, 2023. https://doi.org/10.1080/10407782.2022.2101809

[50] A. Y. U. Mohammad Nawaz Khan, Munawwar Nawab Karimi, "A comprehensive analysis of a rectangular microchannel heat sink furnished with a circular perforated cylindrical pinfin," Numer. Heat Transf. Part A Appl. An Int. J. Comput. Methodol., vol. 85, no. 13, 2024. https://doi.org/10.1080/10407782.2023.2219827

[51] T. Ambreen and M. H. Kim, "Effect of fin shape on the thermal performance of nanofluid-cooled micro pin-fin heat sinks," Int. J. Heat Mass Transf., vol. 126, pp. 245–256, 2018. https://doi.org/10.1016/j.ijheatmasstransfer.2018.05.164.

[52] S. L. Wang, X. Y. Li, X. D. Wang, and G. Lu, "Flow and heat transfer characteristics in double-layered microchannel heat sinks with porous fins," Int. Commun. Heat Mass Transf., vol. 93, pp. 41–47, 2018. https://doi.org/10.1016/j.icheatmasstransfer.2018.03.003.

[53] S. V. Jadhav, P. M. Pawar, and B. P. Ronge, "Effect of pin-fin geometry on microchannel performance," Chem. Prod. Process Model., vol. 14, no. 1, 2019. https://doi.org/10.1515/cppm-2018-0016.

[54] S. Z. Shuja, B. S. Yilbas, and H. Al-Qahtani, "Influence of Hydrophobic Fin Configuration in Thermal System in Relation to Electronic Device Cooling Applications," Energies, vol. 13, no. 7, p. 1631, Apr. 2020. https://doi.org/10.3390/en13071631.

[55] P. Bhandari and Y. K. Prajapati, "Thermal performance of open microchannel heat sink with variable pin fin height," Int. J. Therm. Sci., vol. 159, no. August 2019, p. 106609, 2021. https://doi.org/10.1016/j.ijthermalsci.2020.106609.

[56] O. A. Ismail, A. M. Ali, M. A. Hassan, and O. Gamea, "Geometric optimization of pin fins for enhanced cooling in a microchannel heat sink," Int. J. Therm. Sci., vol. 190, no. December 2022, p. 108321, 2023. https://doi.org/10.1016/j.ijthermalsci.2023.108321.

[57] Y. Yan, J. Wu, F. Xu, Y. Chen, and Z. He, "Experimental investigation on flow and heat transfer characteristics of the drop-pressure microchannel heat sink with gradient distribution pin fin arrays and narrow slots," Appl. Therm. Eng., vol. 233, p. 121084, 2023. https://doi.org/https://doi.org/10.1016/j.applthermaleng.2023.121084.

[58] M. Alam, M. Nawaz Khan, D. Ansari, K. Rasheed, P. Kumar Bharti, and A. Dwivedi, "Performance analysis of microchannel heat sink with ribbed pinfins," Int. J. Heat Fluid Flow, vol. 109, no. May, p. 109529, 2024. https://doi.org/10.1016/j.ijheatfluidflow.2024.109529.

[59] A. Manoj, U. V. Goddumarri, R. A, and S. Chakraborty, "Heat transfer and fluid flow characteristics of a microchannel heat sink with microplates - A critical computational study," Appl. Therm. Eng., vol. 226, no. February, p. 120309, 2023. https://doi.org/10.1016/j.applthermaleng.2023.120309.

[60] S. L. Sun, D. Liu, Y. Z. Wang, H. B. Kim, M. Hassan, and H. J. Hong, "Heat transfer performance prediction of Taylor–Couette flow with longitudinal slits using artificial neural networks," Appl. Therm. Eng., vol. 221, no. June 2022, p. 119792, 2023. https://doi.org/10.1016/j.applthermaleng.2022.119792.

[61] S. Nekahi, F. Sadegh Moghanlou, K. Vaferi, H. Ghaebi, M. Vajdi, and H. Nami, "Optimizing finned-microchannel heat sink design for enhanced overall performance by three different approaches: Numerical simulation, artificial neural network, and multi-objective optimization," Appl. Therm. Eng., vol. 245, p. 122835, May 2024. https://doi.org/10.1016/j.applthermaleng.2024.122835.

[62] A. Rabiee, M. Ahmadian-Elmi, M. R. Hajmohammadi, and M. Mohammadifar, "Multi-objective optimization of rectangular microchannel heat sink based on entropy generation and hydro-thermal performance using NSGA-II algorithm," Int. Commun. Heat Mass Transf., vol. 149, no. November, p. 107140, 2023. https://doi.org/10.1016/j.icheatmasstransfer.2023.107140.

[63] W. Qu and I. Mudawar, "Experimental and numerical study of pressure drop and heat transfer in a single-phase micro-channel heat sink," 2002. https://doi.org/10.1016/S0017-9310(01)00337-4

[64] S. Alimohammadi, D. B. Murray, and T. Persoons, "Experimental validation of a computational fluid dynamics methodology for transitional flow heat transfer characteristics of a steady impinging jet," J. Heat Transfer, vol. 136, no. 9, pp. 1–10, 2014. https://doi.org/10.1115/1.4027840.